

LIST OF TABLES

<u>CHAPTERS</u>	<u>TABLE CAPTIONS</u>	<u>PAGE NO.</u>
Chapter-II	Table II.1: Characteristics of Cyclodextrin.	39
Chapter-IV	Table IV.1: Molar Conductance (Λ) and Surface tension (γ) values with corresponding concentration at the CMC and saturation point of inclusion; and concentration ratio (ratio of inclusion IL: β -CD) at the break point of the surfactants solution (0.01 M) in aqueous β -CD	141
	Table IV.2: Free energy of micellization (ΔG_{mic}) and free energy of change (ΔG) obtained from degree of micelle ionization (α) and association constant (K_a) of the solution (β -CD+ionic liquid) at 25°C evaluated from the conductance and surface tension measurement respectively	142
Chapter-V	Table V.1: Values of observed molar conductivities (Λ) at various mole ratios for the system Amantadine-18C6 at different temperature	157-158
	Table V.2: Values of formation constant, enthalpy, entropy and free energy change of amantadine-18C6 complex in methanol solution	160
	Table V.3: Experimental values of surface tension (γ) corresponding to concentration of 18C6 in methanolic solution	161
	Table V.4: Values of surface tension (γ) at the break point with corresponding to concentration of 18C6 in methanolic solution at 298.15 K	163
	Table V.5: Experimental values of density (ρ) in different mass fraction of methanolic solution of 18C6	164
	Table V.6: Experimental values of densities (ρ) corresponding to concentration in different mass fractions of methanolic solution of 18C6 at different temperature	165

	Table V.7: Limiting apparent molar volume (ϕ_v^0) and experimental slope (S_v^*) in different mass fractions of methanolic solution of 18-crown-6	165-166
	Table V.8: Limiting apparent molar expansibilities (ϕ_E^0) for amantadine hydrochloride in different mass fraction of 18C6 in methanol solution (w_1) at 298.15K to 308.15K respectively	168
Chapter VI	Table VI.1: Density (ρ), viscosity (η) and relative permittivity (ϵ) of the different solvents Acetonitrile, Tetrahydrofuran and Dichloromethane	174
	Table VI.2: The concentration (m) and molal conductance (Λ) of [bmim][Cl] in Acetonitrile, Dichloromethane and Tetrahydrofuran at 298.15 K, 303.15K and 308.15K respectively	175-176
	Table VI.3: Limiting molar conductance (Λ_0), association constant (K_A), co-sphere diameter (R) and standard deviations of experimental Λ (δ) obtained from Fuoss conductance equation of [bmim][Cl] in Acetonitrile at 298.15 K, 303.15 K and 308.15 K respectively	178
	Table VI.4: Walden product ($\Lambda_0 \cdot \eta$) and Gibb's energy change (ΔG°) of [bmim][Cl] in Acetonitrile at 298.15 K, 303.15 K and 308.15 K respectively	179
	Table VI.5: Limiting Ionic Conductance (λ_0^\pm), Ionic Walden Product ($\lambda_0^\pm \eta$), Stokes' Radii (r_s), and Crystallographic Radii (r_c) of [bmim][Cl] in Acetonitrile at 298.15 K, 303.15 K and 308.15 K respectively	179
	Table VI.6: Thermodynamic parameters for [bmim][Cl] in ACN	180
	Table VI.7: The calculated limiting molar conductance of ion-pair (Λ_0), limiting molar conductances of triple ion Λ_0^T , experimental slope and intercept obtained from Fuoss-Kraus Equation for [bmim][Cl] in DCM and THF at 298.15 K, 303.15 K and 308.15 K respectively	183

	<p>Table VI.8: Salt concentration at the minimum conductivity (C_{min}) along with the ion-pair formation constant (K_P), triple ion formation constant (K_T) for [bmim][Cl] in DCM and THF at 298.15 K, 303.15 K and 308.15 K respectively</p>	184
	<p>Table VI.9: Salt concentration at the minimum conductivity (C_{min}), the ion pair fraction (α), triple ion fraction (α_T), ion pair concentration (C_P) and triple-ion concentration (C_T) for [bmim][Cl] in DCM and THF at 298.15 K, 303.15 K and 308.15 K respectively</p>	186
	<p>Table VI.10: Density (ρ) and viscosity (η) of 1-butyl-3-methylimidazolium chloride in different mass fraction of Acetonitrile, Dichloromethane and Tetrahydrofuran at different temperatures</p>	187-188
	<p>Table VI.11: Apparent molal volume (ϕ_V) and $\frac{(\eta_r - 1)}{\sqrt{m}}$ for 1-butyl-3-methylimidazolium Chloride ([bmim][Cl]) in different mass fraction of Acetonitrile, Dichloromethane and Tetrahydrofuran at different temperatures</p>	189
	<p>Table VI.12: Limiting apparent molar volume (ϕ_V^0), experimental slope (S_V^*), viscosity B-and viscosity A- coefficient for [bmim][Cl] in ACN, DCM and THF at T= (298.15 to 308.15) K respectively</p>	190
	<p>Table VI.13: Values of empirical coefficients (a_0, a_1, and a_2) of Equation 26 of the [bmim][Cl] in ACN, DCM and THF</p>	192
	<p>Table VI.14: Limiting apparent molal expansibilities (ϕ_E^0) of [bmim][Cl] in ACN, DCM and THF at T= (298.15 to 308.15) K</p>	193
	<p>Table VI.15: Stretching frequencies of the functional groups present in the pure solvent and change of frequency after addition of [bmim][Cl] in the solvents</p>	195

Chapter VII	Table VII.1: Data for the Job plot performed by UV-Vis spectroscopy for SA-DC18C6 system	201
	Table VII.2: Data for the Job plot performed by UV-Vis spectroscopy for SA-18C6 system	201
	Table VII.3: Data for the Job plot performed by UV-Vis spectroscopy for SA-DB18C6 system	202
	Table VII.4: Comparison between the Frequencies change (cm^{-1}) of different functional group of free compound and their complexes	205
	Table VII.5: Experimental values of density (ρ) and viscosity (η) of sulfa drug in different mass fraction of DC18C6 (w_1), 18C6 (w_2) and DB18C6 (w_3) in ACN at T= (293.15 to 308.15) K	209-211
	Table VII.6: Limiting apparent molar volume (ϕ_V^0) and viscosity B-coefficient of sulfa drug in different mass fraction of different crown ethers in ACN at T= (293.15 to 308.15) K	213-214
	Table VII.7: Values of empirical coefficients (a_0 , a_1 , and a_2) of Equation 14 of sulfa drug in different mass fraction of DC18C6 (w_1), 18C6 (w_2) and DB18C6 (w_3) in ACN at T= (293.15 to 308.15) K	215
	Table VII.8: Limiting apparent molal expansibilities (ϕ_E^0) of sulfa drug in different mass fraction of DC18C6 (w_1), 18C6 (w_2) and DB18C6 (w_3) in ACN at T= (293.15 to 308.15) K	216
	Table VII.9: Values of dB/dT of sulfa drug in different mass fraction of DC18C6 (w_1), 18C6 (w_2) and DB18C6 (w_3) in ACN at T= (293.15 to 308.15) K respectively	219

	Table VII.10: Values of Refractive Index (n_D) and Molar Refraction (R_M) of sulfa drug in different mass fraction of DC18C6 (w_1), 18C6 (w_2) and DB18C6 (w_3) in ACN at $T=298.15$ K respectively	221-222
	Table VII.11: Limiting molar refractions (R_M^0) values of sulfa drug in different mass fraction of DC18C6 (w_1), 18C6 (w_2) and DB18C6 (w_3) in ACN at $T=298.15$ K respectively	223
	Table VII.12: Values of Association constant (K_a) and free energy change (ΔG^0) of the three SA-CEs complexes	225
	Table VII.13: Data for the Benesi-Hildebrand double reciprocal plot performed by UV-Vis spectroscopy for SA-DC18C6 system	227
	Table VII.14: Data for the Benesi-Hildebrand double reciprocal plot performed by UV-Vis spectroscopy for SA-18C6 system	227
	Table VII.15: Data for the Benesi-Hildebrand double reciprocal plot performed by UV-Vis spectroscopy for SA-DB18C6 system	227
Chapter VIII	Table VIII.1: Data for the Job plot performed by UV-Vis spectroscopy for aqueous MP: α -CD system at $298.15K^a$	234
	Table VIII.2: Data for the Job plot performed by UV-Vis spectroscopy for aqueous MP: β -CD system at $298.15K^a$	235
	Table VIII.3: Data for surface tension and conductivity study of aqueous MP: α -CD system at $298.15K^a$	237
	Table VIII.4: Data for surface tension and conductivity study of aqueous MP: β -CD system at $298.15K^a$	238
	Table VIII.5: Values of surface tension (γ) at the break point with corresponding concentrations of MP and CD at $298.15K^a$	239
	Table VIII.6: Values of conductivity (κ) at the break point with corresponding concentrations of MP and CD at $298.15K^a$	240

	Table VIII.7: Data for the Benesi-Hildebrand double reciprocal plot performed by UV-Vis spectroscopy for MP: α -CD system	241
	Table VIII.8: Data for the Benesi-Hildebrand double reciprocal plot performed by UV-Vis spectroscopy for MP: β -CD system	243
	Table VIII.9: Data for the Benesi-Hildebrand double reciprocal plot performed by fluorescence spectroscopy for MP: α -CD system	244
	Table VIII.10: Data for the Benesi-Hildebrand double reciprocal plot performed by fluorescence spectroscopy for MP: β -CD system	245
	Table VIII.11: Values of Association constants (K_a) obtained by Benesi-Hildebrand method both from UV-vis spectroscopy and Fluorescence spectroscopy and corresponding free energy change (ΔG^0) of the MP:CD inclusion complexes at 298.15K ^a	246
	Table VIII.12: Comparison between the Frequencies change (cm^{-1}) of different functional group of free compound and their solid complexes	252-253
Chapter IX	Table IX.1: Values of observed molar conductivities, Λ , at various mole ratios for the system IL-18C6 (complex 1) and IL-DB186 (complex 2) at different temperature	258
	Table IX.2: Values of formation constant, enthalpy, entropy and free energy change of different crown ethers complexes in ACN solution	260
	Table IX.3: Comparison between the Frequencies change (cm^{-1}) of different functional group of free compound and their complexes	266

LIST OF FIGURES

<u>CHAPTERS</u>	<u>FIGURE CAPTIONS</u>	<u>PAGE NO.</u>
Chapter-II	Figure II.1: Schematic representation for host-guest complexation by Cyclodextrin	35
	Figure II. 2: Schematic representation of various interactions involved in host-guest chemistry	36
	Figure II. 3: From molecular to supramolecular chemistry	36
	Figure II. 4: Structures of the α -, β - and γ -cyclodextrin	38
	Figure II. 5: General structure of cyclodextrin molecule with interior and exterior protons ($n = 6, 7$ for α -CD and β -CD respectively)	39
	Figure II.6: Different stoichiometries of host-guest inclusion complexes	41
	Figure II.7: Schematic drawing of cation- π interactions showing the contact of K^+ ion and benzene	43
	Figure II.8: Several example of crown ethers	44
	Figure II.9: Pedersen's reaction	45
	Figure II.10: Growth rate of ionic liquid publications, 1986-2006	54
	Figure II.11: Annual growth of ionic liquid patents, 1996-2006	55
	Figure II.12: A diagram for the explanation of molal volume.	64
Chapter-IV	Figure IV.1: Plot of surface tension (γ) with corresponding conc. (M) of ionic liquids	140
	Figure IV.2: Plot of molar conductance (Λ) with corresponding conc. (M) of ionic liquids	142
	Figure IV.3: Plot of surface tension (γ) of ionic liquids (0.01M) with corresponding conc.(M) of β -CD	143
	Figure IV.4: Plot of molar conductance (Λ) of ionic liquids (0.01M) with corresponding conc. (M) of β -CD	144
	Figure IV.5: Plot of surface tension (γ) with corresponding conc. of ionic liquids in absence (solid fill) and in presence (no fill) of β -CD	145

	Figure IV.6: (a) Stereo-chemical configuration, (b) truncated conical structure of β -cyclodextrin with interior and exterior protons	148
	Figure IV.7: ^1H NMR spectra of (a) β -CD, (b) $[(\text{C}_6\text{H}_5\text{CH}_2)\text{N}(\text{CH}_3)_3]\text{Cl}$, and (c) inclusion complex	148
	Figure IV.8: ^1H NMR spectra of (a) β -CD, (b) $[(\text{C}_6\text{H}_5\text{CH}_2)\text{N}(\text{C}_2\text{H}_5)_3]\text{Cl}$, and (c) inclusion complex	149
	Figure IV.9: ^1H NMR spectra of (a) β -CD, (b) $[(\text{C}_6\text{H}_5\text{CH}_2)\text{N}(\text{C}_4\text{H}_9)_3]\text{Cl}$, and (c) inclusion complex.	149
	Figure IV.10: Relationship between (S_o-S) and $(S_o/S)-1$ for solution of ionic liquids along and mixed with β -CD	150
Chapter-V	Figure V.1: A space filling model of 18-crown-6 showing the open space at the center of the crown and electron pairs present on the exposed oxygen atoms (in pink)	155
	Figure V.2: Molar conductance vs $[18\text{C}6]/[\text{amantadine ion}]$ at 298.15 K (\blacktriangle), 303.15 K (\boxtimes), 308.15 K (\bullet)	157
	Figure V.3: The linear relationship of $\log K_f$ vs $1/T$ for the interaction between amantadine hydrochloride with 18C6	159
	Figure V.4: Variation of surface tension of amantadine with increasing concentration of 18C6 at 298.15 K	162
	Figure V.5: FTIR spectra of pure amantadine hydrochloride (black), 18-crown-6 (blue) and complex (red)	163
	Figure V.6: Plot of limiting apparent molar volume (φ_v°) of amantadine against different temperature (298.15 K, 303.15 K, 308.15 K) in mass fractions $w_1=0.001$ (\blacksquare), $w_1=0.004$ (\blacksquare), $w_1=0.007$ (\blacksquare) mass fractions of 18C6 in methanol solution	166
Chapter VI	Figure VI.1: Plot of molar conductance (Λ) versus \sqrt{m} of $[\text{bmim}][\text{Cl}]$ in ACN at 298.15 K (\blacklozenge), 303.15 K (\bullet) and 308.15 K (\blacktriangle)	175
	Figure VI.2: The linear relationships of $\ln K_a$ vs. $1/T$ for the ion pair formation in ACN	181

	Figure VI.3: Plot of molar conductance (Λ) versus \sqrt{m} for [bmim][Cl] in DCM at 298.15 K (\blacklozenge), 303.15 K (\bullet) and 308.15 K (\blacktriangle) and in THF at 298.15 K (\blacklozenge), 303.15 K (\circ) and 308.15 K (\blacktriangle)	182
	Figure VI.4: Plot of limiting apparent molal volume (ϕ_V^0) versus temperature for [bmim][Cl] in ACN (yellow), DCM (green) and THF (blue)	191
	Figure VI.5: Plot of viscosity B-coefficient versus temperature for [bmim][Cl] in ACN (blue), DCM (red) and THF (green)	194
Chapter VII	Figure VII.1: Job plot of (a) SA-DC18C6 system, (b) SA-18C6 system, (c) SA-DB18C6 system at T= 298.15 K	200
	Figure VII.2: FTIR spectra of free DC18C6 (Black), SA (Blue) and complex 1 (Red)	203
	Figure VII.3: FTIR spectra of free 18C6 (Black), SA (Blue) and complex 2 (Red)	203
	Figure VII.4: FTIR spectra of free DB18C6 (Black), SA (Blue) and complex 3 (Red)	204
	Figure VII.5: The ^1H NMR spectra of complex 1 (SA-DC18C6) (upper), uncomplexed SA and DC18C6 (lower) recorded at 300 MHz in CD_3CN at 298.15 K	206
	Figure VII.6: The ^1H NMR spectra of complex 2 (SA-18C6) (upper), uncomplexed SA and 18C6 (lower) recorded at 300 MHz in CD_3CN at 298.15 K	207
	Figure VII.7: The ^1H NMR spectra of complex 3 (SA-DB18C6) (upper), uncomplexed SA and DB18C6 (lower) recorded at 300 MHz in CD_3CN at 298.15 K	207
	Figure VII.8: Plot of limiting apparent molar volume (ϕ_V^0) of SA in mass fractions (a) 0.001, (b) 0.003, (c) 0.005 (w) of different CEs in ACN at T= (293.15 to 308.15)K respectively	212

	Figure VII.9: Plot of viscosity B-coefficient of SA in mass fractions (a) 0.001, (b) 0.003, (c) 0.005 (w) of different CEs in ACN at T= (293.15 to 308.15)K respectively	218
	Figure VII.10: Plot of limiting molar refraction (R_M^0) of SA in different mass fractions (w) of different CEs in ACN at T= 298.15 K respectively	220
	Figure VII.11: Benesi-Hildebrand double reciprocal plot for the effect of (a) DC18C6, (b) 18C6, (c) DB18C6 on the absorbance of Sulfa drug	226
Chapter VIII	Figure VIII.1: Job plots of (a) MP: α -CD system and (b) MP: β -CD system at $\lambda_{max} = 272$ nm at 298.15 K. $R = [SS]/([MP] + [CD])$, $\Delta A =$ absorbance difference of MP with and without CD	234
	Figure VIII.2: Variation of surface tension of aqueous MP with increasing concentration of (a) α -CD and (b) β -CD solution respectively at 298.15 K.	236
	Figure VIII.3: Variation of surface tension of aqueous MP with increasing concentration of (a) α -CD and (b) β -CD solution respectively at 298.15 K.	239
	Figure VIII.4: (a) Absorption spectra of MP (50 μ M) in different α -CD concentrations (μ M): 1) without α -CD, 2) 30 μ M, 3) 40 μ M, 4) 50 μ M, 5) 60 μ M, 6) 70 μ M. (b) Benesi-Hildebrand plot of $1/A - A_0$ vs. $1/[\alpha\text{-CD}]$ for 1:1 complexation of MP with α -CD	241
	Figure VIII.5: (a) Absorption spectra of MP (50 μ M) in different β -CD concentrations (μ M): 1) without β -CD, 2) 30 μ M, 3) 40 μ M, 4) 50 μ M, 5) 60 μ M, 6) 70 μ M. (b) Benesi-Hildebrand plot of $1/A - A_0$ vs. $1/[\beta\text{-CD}]$ for 1:1 complexation of MP with β -CD.	242
	Figure VIII.6: (a) Fluorescence emission spectra of MP (5 μ M) in different α -CD concentrations (μ M): 1) without α -CD, 2) 10 μ M, 3) 20 μ M, 4) 30 μ M, 5) 40 μ M, 6) 50 μ M. (b) Benesi-Hildebrand plot of $1/I - I_0$ vs. $1/[\alpha\text{-CD}]$ for 1:1 complexation of MP with α -CD.	244

	Figure VIII.7: (a) Fluorescence emission spectra of MP (5 μM) in different $\beta\text{-CD}$ concentrations (μM): 1) without $\beta\text{-CD}$, 2) 10 μM , 3) 20 μM , 4) 30 μM , 5) 40 μM , 6) 50 μM . (b) Benesi–Hildebrand plot of $1/I - I_0$ vs. $1/[\beta\text{-CD}]$ for 1:1 complexation of MP with $\beta\text{-CD}$	245
	Figure VIII.8: ^1H NMR spectra of (a) $\alpha\text{-CD}$, (b) MP and (c) 1:1 M ratio of $\alpha\text{-CD}$ & MP in D_2O at 298.15 K.	247
	Figure VIII.9: ^1H NMR spectra of (a) $\beta\text{-CD}$, (b) MP and (c) 1:1 M ratio of $\beta\text{-CD}$ & MP in D_2O at 298.15 K	247
	Figure VIII.10: FTIR spectra of free $\alpha\text{-CD}$, MP and their 1:1 inclusion complex (MP: $\alpha\text{-CD}$)	251
	Figure VIII.11: FTIR spectra of free $\beta\text{-CD}$, MP and their 1:1 inclusion complex (MP: $\beta\text{-CD}$)	251
Chapter IX	Figure IX.1: Molar conductance vs $[\text{18C6}]/[\text{cation}]$ at 298.15 K (\blacktriangle), 303.15 K (\blacksquare), 308.15 K (\bullet)	261
	Figure IX.2: Molar conductance vs $[\text{DB18C6}]/[\text{cation}]$ at 298.15 K (Δ), 303.15 K (\square), 308.15 K (\circ)	261
	Figure IX.3: The linear relationship of $\log K_f$ vs. $1/T$ for the interaction of IL with 18C6 (\bullet) and DB18C6 (\blacksquare).	263
	Figure IX.4: FTIR spectra of free IL (Black), 18-crown-6 (Blue) and complex (Red)	265
	Figure IX.5: FTIR spectra of free IL (Black), Dibenzo-18-crown-6 (Blue) and complex (Red).	265
	Figure IX.6: The ^1H NMR spectra of complex 1 (18C6.IL) (upper) and uncomplexed imidazolium cation (lower) recorded at 300 MHz in CD_3CN at 298.15 K	268
	Figure IX.7: The ^1H NMR spectra of complex 2 (DB18C6.IL) (upper) and uncomplexed imidazolium cation (lower) recorded at 300 MHz in CD_3CN at 298.15 K	268

LIST OF SCHEMES

<u>CHAPTERS</u>	<u>SCHEME CAPTIONS</u>	<u>PAGE NO.</u>
Chapter-IV	Scheme IV.1: <i>Molecular structure of cationic surfactant and β-cyclodextrin</i>	138
	Scheme IV.2: <i>Schematic illustration of plausible micelle (2a), distraction of micelle (2b) and plausible inclusion formation (2c).</i>	145
	Scheme IV.3: <i>Schematic representation of mechanism of formation of inclusion complexes of cationic ionic liquids with β-cyclodextrin</i>	146
	Scheme IV.4: <i>Schematic representation of inclusion complexes of cationic ionic liquids with β-cyclodextrin</i>	147
Chapter-V	Scheme V.1: <i>Molecular structure of Amantadine hydrochloride and 18C6</i>	154
	Scheme V.2: <i>Schematic presentation of complexation between amantadine ion and 18C6 and corresponding energy minimized structure of the complex</i>	162
Chapter-VI	Scheme VI.1: <i>Molecular structures of the IL and the solvents</i>	172
	Scheme VI.2: <i>Pictorial representation of ion-pair and triple-ion formation for the electrolyte in diverse solvent systems</i>	185
	Scheme VI.3: <i>Extent of ion-solvent interaction of IL in various solvent systems</i>	191
Chapter-VII	Scheme VII.1: <i>Molecular structure of crown ethers and SA</i>	198
	Scheme VII.2a: <i>Schematic presentation of complex formation between SA and DC18C6 and corresponding energy minimized structure of the complex</i>	223-224
	Scheme VII.2b: <i>Schematic presentation of complex formation between SA and 18C6 and corresponding energy minimized structure of the complex</i>	
	Scheme VII.2c: <i>Schematic presentation of complex formation between SA and DB18C6 and corresponding energy minimized structure of the complex</i>	

<u>CHAPTERS</u>	<u>SCHEME CAPTIONS</u>	<u>PAGE NO.</u>
Chapter-VIII	<i>Scheme VIII.1:</i> Molecular structures of (a) metoclopramide hydrochloride and (b) cyclodextrin molecule with interior and exterior protons ($n = 6, 7$ for α -CD and β -CD respectively)	231
	<i>Scheme VIII.2:</i> Plausible schematic presentation of mechanism for formation of 1:1 inclusion complex between metoclopramide hydrochloride and cyclodextrin	248
Chapter-IX	<i>Scheme IX.1:</i> Molecular structure of crown ethers and IL	256
	<i>Scheme IX.2:</i> Plausible schematic presentation of complex formation between imidazolium cation and crown ethers	259

LIST OF APPENDICES

- ✓ **Appendix A:** List of Publications/Communications
- ✓ **Appendix B:** List of Seminars / Symposiums/
Conferences Attended
- ✓ **Appendix C:** List of abbreviation and symbol

APPENDIX-A

LIST OF RESEARCH PUBLICATION(S)

- [1] NMR, Surface tension and Conductance Study to Investigate Host-guest Inclusion Complexes of Three Sequential Ionic Liquids with β -cyclodextrin in Aqueous Media



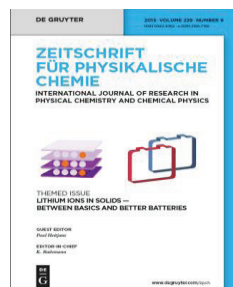
Chemical Physics Letters

658 (2016) 43–50.

(Included in the Thesis)



- [2] Investigation Probing Inclusion Complex Formation of Amantadine Hydrochloride with 18-Crown-6 in Methanol by Physicochemical Approach



Zeitschrift für Physikalische Chemie

231 (2016) 1111-1126.

(Included in the Thesis)



- [3] Investigation on Solvation Behavior of an Ionic Liquid (1-butyl-3-methylimidazolium chloride) with the Manifestation of Ion Association Prevailing in Different Pure Solvent Systems



*Indian Journal of Advances in
Chemical Science*
5 (2017) 1-16.

(Included in the Thesis)



- [4] Interactions of an Antifungal Sulfa Drug with Diverse Macrocyclic Polyethers Explaining Mechanism, Performance and Physiognomies Leading to Formation of Stable Complexes

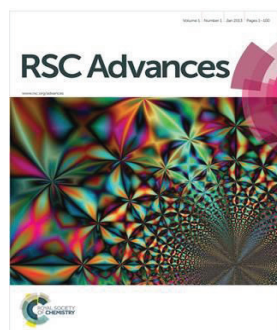
Communicated

(Included in the Thesis)

- [5] Subsistence of Host-Guest Inclusion Complexes of Metoclopramide Hydrochloride with α - and β -Cyclodextrin Molecules Probed by Physicochemical Investigation

Communicated

(Included in the Thesis)

[6] Hollow Circular Compound-Based Inclusion Complexes of an Ionic Liquid

RSC Advances
6 (2016) 76381-76389.

(Included in the Thesis)

**[7]** Self Assembly Inclusion of Ionic Liquid into Hollow Cylinder Oligosaccharides

Journal of Molecular Liquids
214 (2016), 264-269.



- [8] Study on Diverse Interactions of Vitamin Molecules Insight into $\text{H}_2\text{O} + [\text{Epy}]\text{BF}_4$ Systems by Physicochemical Contrivance



*Indian Journal of Advances
in Chemical Science*
3 (2015) 204-218.



- [9] Exploration of Inclusion Complexes of Neurotransmitters with β -Cyclodextrin by Physicochemical Techniques



Chemical Physics Letters
655-656 (2016), 43-50.



- [10] Host-guest Inclusion Complexes of RNA Nucleosides inside aqueous Cyclodextrins Explored by Physicochemical and Spectroscopic Methods



RSC Advances
6 (2016) 8881-8891.



APPENDIX-B

LIST OF SEMINARS/ SYMPOSIUMS/ CONFERENCES ATTENDED

1. **National Seminar on Frontiers in Chemistry - 2014** Sponsored by University Grants Commission (SAP-DRS-III), New Delhi, organized by Department of Chemistry, University of North Bengal on March 11th & 12th, 2014.
2. **Science Academies' Lecture Workshop on "Spectroscopy of Emerging Materials"** organised by the Department of Chemistry, University of North Bengal on November 26th & 27th, 2014.
3. **National Seminar on Frontiers in Chemistry - 2015** Funded by University Grants Commission and SAP (DRS-III) New Delhi, organized by the Department of Chemistry, University of North Bengal on February 17th & 18th, 2015.
4. **22nd West Bengal State Science & Technology Congress-2015** Organized by Department of Science and Technology, Govt. of West Bengal, West Bengal State Council of Science and Technology and University of North Bengal, Raja Rammohanpur, Darjeeling-734013 on February 28th & March 1st, 2015.
5. **Recent Trends on Chemistry and Biology Interface-2015** Organized by Chemical Research Society of India, NBU-Local Chapter, Department of Chemistry, University of North Bengal (Darjeeling) on August 28, 2015.
6. **19th CRSI National Symposium in Chemistry-2016** Organized by Department of Chemistry, University of North Bengal, Raja Rammohanpur, Darjeeling-734013 on July 14th to 16th, 2016.
7. **20th CRSI National Symposium in Chemistry-2017** Organized by Department of Chemistry, Gauhati University, Guwahati on February 3rd to 5th, 2017.
8. **Current Trends in University- Industries Linkages-2017** Funded by University Grants Commission and Organized by Department of Chemistry, University of North Bengal, Darjeeling-734013, W.B, India on 24th March, 2017.

APPENDIX: C

LIST OF ABBREVIATION

ACN	Acetonitrile
ADH	Amantadine Hydrochloride
[bmim][Cl]	1-butyl-3-methylimidazolium Chloride
CMC	Critical Micellar Concentration
CH ₃ OH	Methanol
CD	Cyclodextrin
α -CD	α -cyclodextrin
β -CD	β -cyclodextrin
CEs	Crown Ethers
18C6	18-crown-6
DB18C6	Dibenzo-18-crown-6
DC18C6	Dicyclohexyl-18-crown-6
°C	Degree Celcius
DCM	Dichloromethane
FTIR	Fourier Transform Infra-red Spectroscopy
ILs	Ionic liquids
M	Molarity
mL	Milli Litre
mM	Milli Molar
mPa	Milli Pascal
MP	Metoclopramide hydrochloride
¹ H-NMR	Proton-Nuclear Magnetic Resonance
RI	Refractive Index
Str.	Stretching
SA	Sulfanilamide
THF	Tetrahydrofuran
UV	Ultra Violet

LIST OF SYMBOL

ρ	Density
ϕ_V	Apparent molar volume
ϕ_V^0	Limiting apparent molar volume
S_V^*	Experimental slopes
ϕ_E^0	Limiting apparent molar expansibilities
η	Viscosity of the solution
η_0	Viscosity of the solvent
$\eta_r = \eta / \eta_0$	Relative viscosity
Λ	Molar conductance
Λ_0	Limiting molar conductance
ϵ	Relative permittivity of the solvent
$\Lambda_0 \eta$	Walden product
λ_0^\pm	Ionic limiting molar conductances
$\lambda_0^\pm \eta$	Limiting ionic Walden product
r_s	Stokes' radii
r_c	Crystallographic Radii
K_A	Association constant
R	Distance of closest approach
$a = (r_+ + r_-)$	Sum of the crystallographic radii of the cation (r_+) and anion (r_-)
d	Average distance corresponding to the side of a cell occupied by a solvent molecule
$\lambda_0^\pm \eta$	The limiting ionic Walden product
E_a	Activation energy
T	Absolute temperature
K_p	Ion-pair formation constant
K_T	Triple-ion formation constant
C_p	Ion-pair concentrations
C_T	Triple-ion concentrations
α	Fraction of ion-pairs present in the solutions
α_T	Fraction of triple-ions present in the solutions.